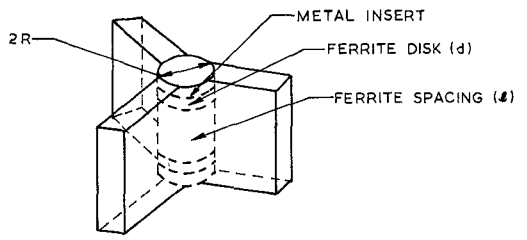

Fig. 1. Schematic of E-plane circulator.

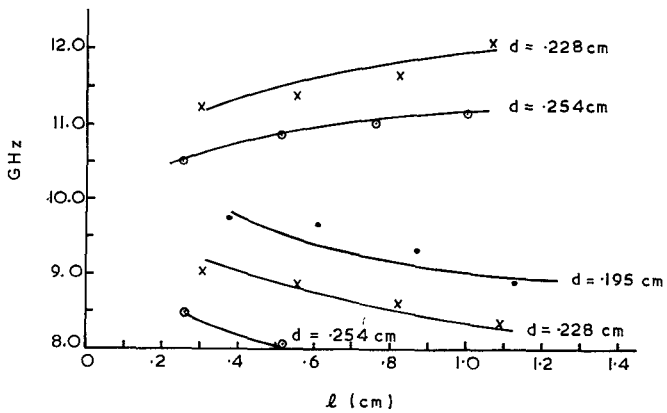

Fig. 2. Mode chart of 3-port junction containing unmagnetized disks.

is a minimum. Mode charts may, therefore, be constructed by determining the frequency at which the VSWR is exactly 2. This approach, although well known, appears to be little used in the formal literature of junction circulators [8], [9]. Its simplicity will be demonstrated in this contribution in connection with the adjustment of the E-plane circulator.

The geometry used is shown in Fig. 1. This geometry has been studied in [2], [3], and [7]. It consists of two ferrite disks placed against the narrow walls at the plane of symmetry of a symmetrical 3-port E-plane waveguide junction. The two variables used to obtain the mode chart were the ferrite thickness and the spacing between the two disks. The spacing between the ferrite disks was adjusted by introducing metal inserts as shown in Fig. 1. The thickness of the metal disks does not appear as a variable in the mode chart because the frequency of the junction is only determined by l, d, and R. The diameter of the ferrite disk was held constant at 1.20 cm. The inside dimensions of the X-band waveguide used were 2.286 by 1.016 cm. The mode charts were plotted over the full frequency range appropriate to the waveguide size. The material used was a garnet one with a saturation magnetization of 0.16 Wb/m^2 and a relative dielectric constant of 15.1.

The relation between the frequency and the spacing between the two ferrite disks for parametric values of ferrite thickness is shown in Fig. 2. It is seen from this illustration that two modes are obtained within the X-band frequency range. The frequency of one mode decreases as the spacing between the two ferrite disks increases. The frequency of the other one increases as the spacing increases. Both modes become independent of ferrite spacing when the spacing is large. It is also seen that the frequency of each mode is proportional to ferrite thickness.

Fig. 3 shows the performance of a circulator obtained by simply magnetizing the first mode using ferrite disks 0.195 cm thick spaced 0.87 cm apart. The magnetic field used was about 3100 A/m. The center frequency obtained with this arrangement is 9.40 GHz which is in close agreement with the prediction of the mode chart. The bandwidth of the resultant circulator is about 400 MHz wide at the 20-dB points. The insertion loss between ports 1 and 2 is 0.40 dB. It should be emphasized that equally good performance can be obtained anywhere on the mode chart.

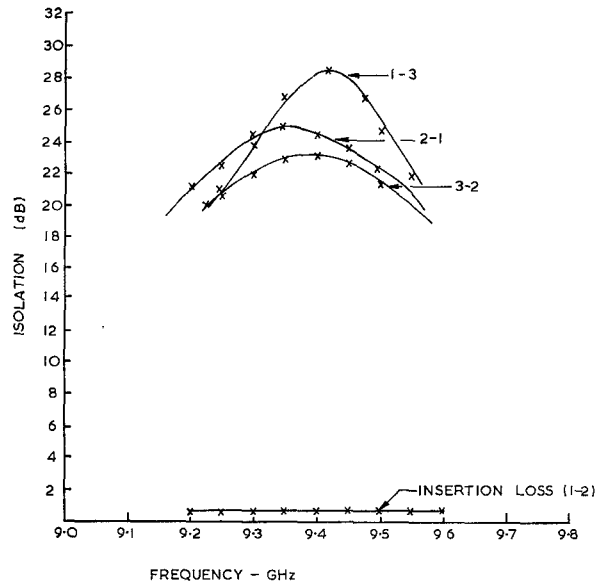

Fig. 3. Frequency response of E-plane circulator using first circulation mode.

The circulator obtained by magnetizing the other mode using the same geometry was one in which circulation occurred in the opposite direction. A similar result has been mentioned in [3].

Acknowledgment

The authors wish to thank T. Wood (Microwave and Electronic Systems Ltd., Lochend Industrial Estate, Midlothian, Scotland) for making the measurements.

References

[1] S. Yoshida, "E-type T circulator," *Proc. IRE* (Corresp.), vol. 47, p. 2018, Nov. 1959.
[2] J. Q. Owen, "E-plane T circulator," Raytheon Co., Waltham, Mass., Unpublished Memo., 1962.
[3] L. E. Davis and S. R. Longley, "E-plane 3-port X-band waveguide circulators," *IEEE Trans. Microwave Theory Tech.*, vol. MTT-11, pp. 443–445, Sept. 1963.
[4] G. Buchta, "Miniaturized broadband E-tee circulator at X-band," *Proc. IEEE* (Lett.), vol. 54, pp. 1607–1608, Nov. 1966.
[5] J. W. McGrown and W. H. Wright, Jr., "A high power, Y-junction, E-plane circulator," in *G-MTT Int. Microwave Symp. Dig.*, p. 85, 1967.
[6] C. E. Fay and R. L. Comstock, "Operation of the ferrite junction circulator," *IEEE Trans. Microwave Theory Tech.*, vol. MTT-13, pp. 15–27, Jan. 1965.
[7] M. Omori, "An improved E-plane waveguide circulator," in *G-MTT Int. Microwave Symp. Dig.*, p. 228, 1968.
[8] B. A. Auld, "The synthesis of symmetrical waveguide circulators," *IRE Trans. Microwave Theory Tech.*, vol. MTT-7, pp. 238–246, Apr. 1959.
[9] J. Helszajn, "Frequency and bandwidth of H-plane TEM junction circulator," *Proc. Inst. Elec. Eng.*, vol. 117, p. 1235, July 1970.

Phase Corrections for Weighted Acoustic Surface-Wave Dispersive Filters

HENRY M. GERARD, G. W. JUDD, AND MELVIN E. PEDINOFF

***Abstract*—Phase errors incurred by a surface acoustic wave propagating through or generated by an apodized interdigital array have been found to cause severe distortions of the filter response. The amount of error is a function of the piezoelectric coupling constant of the delay material and it is found that the distortions are most severe in high-coupling materials. A simple modification to the current method of array design is presented which corrects this phase error. Experimental results for a pulse-compression loop using apodized lithium-niobate surface-wave filters are presented which demonstrate the effectiveness of this method of phase correction.**

Manuscript received April 12, 1971. This work was supported by the U. S. Army Electronics Command, Fort Monmouth, N. J., under Contract DAAB07-71-C-0046.
H. M. Gerard and G. W. Judd are with Hughes Aircraft Company, Ground Systems Group, Fullerton, Calif. 92634.
M. E. Pedinoff is with the Hughes Research Laboratory, Malibu, Calif.

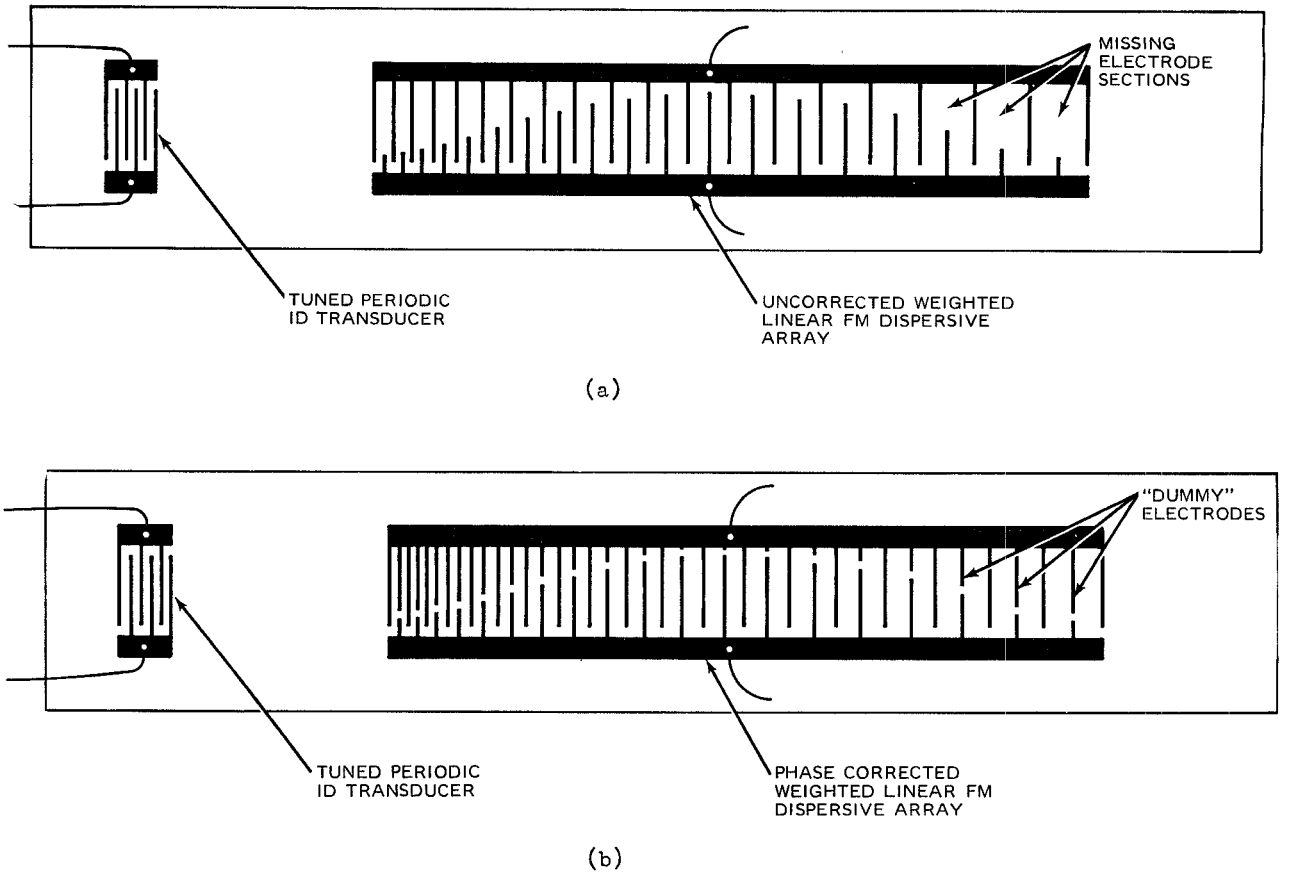

Fig. 1. (a) Typical weighted filter pattern without phase-compensating electrodes. (b) Phase-compensation weighted filter pattern.

Numerous recent efforts have demonstrated the feasibility of using acoustic surface waves in the synthesis of dispersive filters [1], [2]. In general most of the successful results have been obtained using weakly piezoelectric acoustic media, such as quartz. Some degradation in response has been experienced in these filters, however, when amplitude weighting, or apodization, is introduced. The degradation is more severe when strong coupling acoustic media, such as lithium niobate, are used.

This correspondence describes a particular difficulty encountered when the filters are apodized and reports a modification to the array design which led to the successful synthesis of weighted pulse-compression filters on lithium niobate.

Fig. 1(a) shows the electrode pattern for a typical weighted pulse-compression filter. The filter is composed of interdigital electrodes with spacing that varies along the array. An applied RF voltage results in surface-wave generation by the electrodes which are synchronous to the surface wave at the applied frequency. Amplitude weighting can be achieved by apodization, i.e., by varying the overlap distance of the electrodes within the array. The filter in Fig. 1(a) is designed to produce a maximum amplitude signal at the midband frequencies, which correspond to the widest section of the array. The acoustic wave generated in this section propagates along the axis of the array through the region of nonuniformly overlapped electrodes. Wavefront phase distortions occur in this region as a result of the effect of the metal electrodes upon the propagation of the surface wave.

It has been shown that the presence of an electric shorting plane at the surface of a piezoelectric crystal reduces the acoustic surface-wave velocity [3], [4]. The magnitude of the velocity change is proportional to k^2, the effective surface-wave electromechanical coupling constant for the material [5], [6]. It follows that the velocity along an electroded, or partially metallized, piezoelectric surface is similarly reduced the velocity change in this case being determined by both k^2 and the relative extent of the metallization. Differential velocity changes in long interdigital arrays resulting from variable overlap electrode patterns can lead to severe wavefront phase errors in the output signal from these arrays. For example, consider the surface wave excited at the center of the array in Fig. 1(a). The propagation velocity along the midline of the beam is characteristic of one-quarter wavelength shorting strips spaced by one-half wavelength, while the velocity at the beam edge is characteristic of one-quarter wavelength strips spaced by a full wavelength. Since the phase difference between the center and edges of the acoustic beam is proportional to velocity difference and path length, the difference between the velocities need be only a fraction of a percent in order to give large cumulative phase distortions in a long array.

The phase distortions can be prevented by making the array appear to be transversely homogeneous. Fig. 1(b) shows how this can be accomplished without altering the original amplitude weighting scheme. "Dummy" electrodes are inserted into the positions corresponding to missing electrode sections in Fig. 1(a). These electrodes are separated electrically from the active electrodes by small gaps so that no acoustic signal is generated by the "dummy" electrodes. The effective electrode overlap pattern is, therefore, not altered, but the electric shorting effect is made uniform throughout the array.

The use of "dummy" electrodes to correct phase distortion has been demonstrated experimentally. Weighted pulse-expansion and pulse-compression filters were fabricated on y-cut z-axis propagating lithium niobate. One set contained compensating "dummy" electrodes; the other did not. The array patterns were photoetched from a 500-Å thick aluminum film. In subsequent experiments 1000-Å thick patterns were tested and the results were not noticeably different.

The filters had 5-MHz bandwidth centered at 30 MHz with a differential time delay of approximately 4 μs. The expansion filter was designed to generate a linear FM chirp waveform. The matched compression filter incorporated Hamming weighting for sidelobe suppression. Both filters were driven using tuned periodic transducers,

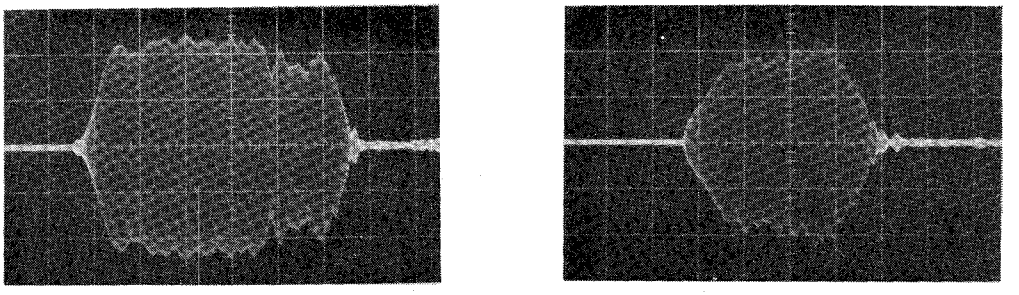

Fig. 2. Measured impulse response of uncompensated expansion and compression filters. (a) Expansion filter. (b) Compression filter.

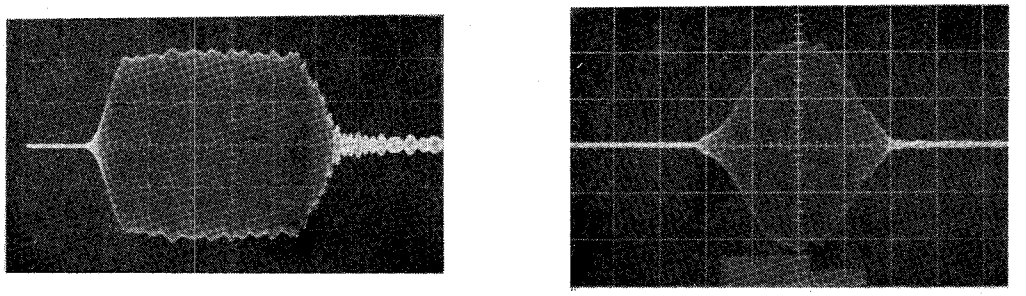

Fig. 3. Measured impulse response of phase-compensated expansion and compression filters. (a) Expansion filter. (b) Compression filter.

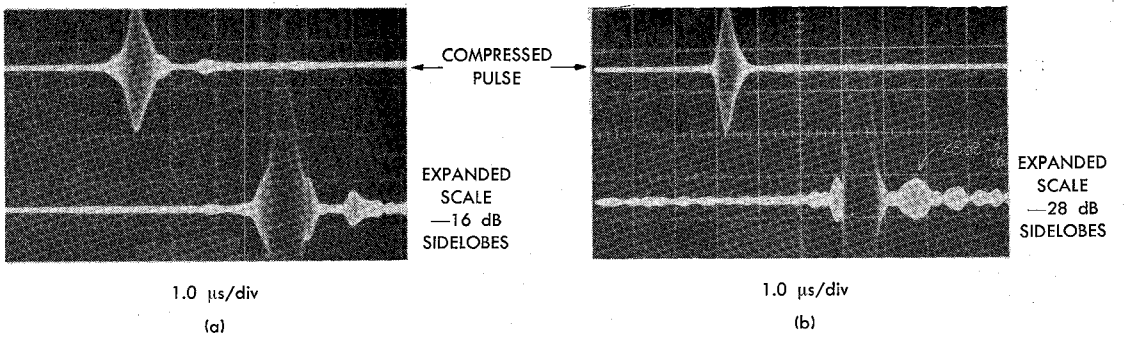

Fig. 4. Recompressed waveform for dispersive filters. (a) Uncompensated. (b) Phase corrected.

as illustrated in Fig. 1(a) and (b). The dispersive array was positioned with the high-frequency end nearest to the periodic transducer, so as to generate a down-chirped waveform in the expansion line and compress an up-chirped signal in the weighted compression line. A mixer was used to spectrally invert the expanded waveform (and thus convert it to an up-chirped signal) prior to compressing it in the weighted compression line.

Fig. 2(a) and (b) show the measured impulse response of the uncorrected expansion and compression filters. Fig. 3(a) and (b) show the corresponding characteristics for the corrected arrays. A relatively small degree of amplitude weighting was required in the expansion filter in order to achieve a flat response. However, considerable weighting was employed in the compression filter for sidelobe suppression. The experimental results indicate that phase compensation improved the response of both the expansion and compression filters. It is also worth noting that the improvement is most dramatic in the filter with the larger variation in electrode overlap distance.

The effectiveness of the phase compensation is demonstrated by the marked improvement in the recompressed waveform produced by the pair of corrected filters as compared to that obtained with the uncompensated filters. Fig. 4(a) shows the compressed pulse produced by the uncorrected filters, and Fig. 4(b) shows the compressed pulse for the phase-corrected pair. No weighting was used in the measurements other than that resulting from the filter apodization. The waveform in Fig. 4(b) illustrates that 28-dB sidelobe suppression is attained in the $\beta\tau = 20$ phase-corrected filters on yz $LiNbO_3$. This represents a 12-dB improvement over the sidelobe level obtained with the uncompensated filters. Furthermore, the midband insertion losses of the expansion and compression filters were measured to be only 20 dB and 15 dB, respectively.

Quantitative data showing the extent of the wavefront phase distortion and the effectiveness of the phase compensation were obtained using an electrical probe technique [7]. The phase profiles of the acoustic output of the compensated and the uncompensated compression filters described above were measured and compared. RF pulses of 2.0-μs duration and near midband frequency were introduced into the apodized arrays, which are shown schematically in Fig. 5(a) and (b). With the aid of a variable phase shifter and a phase detector the acoustic phase at the probe position was measured while the probe was drawn across the acoustic beam. Fig. 5(a) shows the

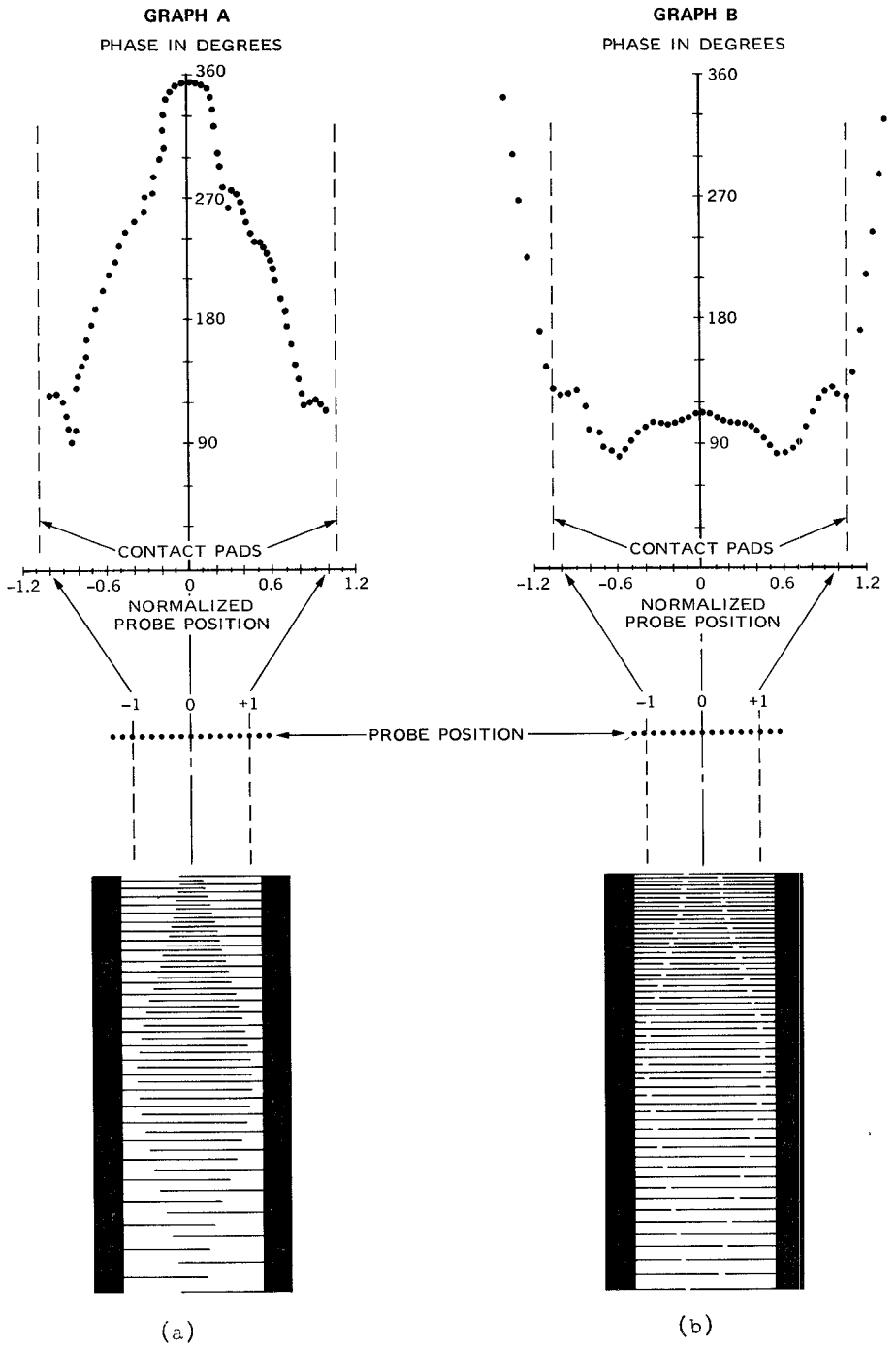

Fig. 5. Measured wavefront phase distortion across the acoustic beam. (a) For uncorrected weighted dispersive filter. (b) For phase-compensated weighted dispersive filter.

measured phase versus probe position for the uncompensated filter. The measurement demonstrates that the phase is not constant over the beam cross section. The decrease in phase away from the midline indicates that the wave velocity increases at the edges of the array pattern. The difference in velocity between the edge and axial acoustic paths in the uncompensated array can be estimated from (1), using the phase data in Fig. 5(a),

$$\frac{v_{\text{edge}} - v_{\text{axial}}}{v} \simeq \frac{(\phi_{\text{axis}} - \phi_{\text{edge}})v}{2\pi f z} \tag{1}$$

where v is the unshorted surface-wave velocity, f is the frequency of excitation, and z is the distance of propagation from the region of excitation (at frequency f) to the end of the array. Using the measured phase difference of 240 degrees and z equal to half the length of the array; i.e., 1 cm, at 30 MHz gives a velocity difference of only about 0.7 percent. The difference in velocity between the *half metallized* axial region and the *one-quarter metallized* edge region is, therefore, approximately one-quarter of the difference between the fully metallized and free surface velocity [4].

The corresponding probe measurement for the phase-compensated array is shown in Fig. 5(b). The data confirm that the use of "dummy" electrodes successfully produce a relatively constant phase across the beam. The phase increases appreciably only near the edges corresponding to acoustic propagation under the contact pads.

The performance of the phase corrected 30-MHz arrays demonstrates that high coupling materials can be used successfully in

surface-wave filter applications. The results indicate, however, that the presence of the electrodes cannot be neglected even at low frequencies where the electrode thickness is negligible compared to the acoustic wavelength. The results further suggest that at high frequencies, where the mass of the electrodes might affect the surface-wave velocity, similar phase-compensating electrodes would be required even in low coupling materials.

References

[1] R. H. Tancrell, M. B. Schultz, H. H. Barrett, L. Davis, Jr., and M. G. Holland, "Dispersive delay lines using ultrasonic surface waves," *Proc. IEEE (Special Issue on Topside Sounding and the Ionosphere)* (Lett.), vol. 57, pp. 1211–1213, June 1969.

[2] L. R. Adkins, W. L. Bongianni, P. J. Hagon, and A. J. Hughes, "Microwave magnetic and acoustic materials, microwave surface wave techniques," ECOM, Ft. Monmouth, N. J., Final Rep. ECOM-0321-F, Dec. 1970.

[3] C. C. Tseng, "Elastic surface waves on free surface and metallized surface of CdS, ZnO and PZT-4," *J. Appl. Phys.*, vol. 38, p. 4281, 1967.

[4] J. J. Campbell and W. R. Jones, "A method for estimating optimal crystal cuts and propagation directions for excitation of piezoelectric surface waves," *IEEE Trans. Sonics Ultrason.*, vol. SU-15, pp. 209–217, Oct. 1968.

[5] W. R. Smith, H. M. Gerard, J. H. Collins, T. M. Reeder, and H. J. Shaw, "Analysis of interdigital surface wave transducers by use of an equivalent circuit model," *IEEE Trans. Microwave Theory Tech. (Special Issue on Microwave Acoustics)*, vol. MTT-17, pp. 856–864, Nov. 1969.

[6] K. A. Ingebrigtsen, "Surface waves in piezoelectrics," *J. Appl. Phys.*, vol. 40, pp. 2681–2686, 1969.

[7] B. A. Richardson and G. S. Kino, "Probing of elastic surface waves in piezoelectric media," *Appl. Phys. Lett.*, vol. 16, pp. 82–84, 1970.

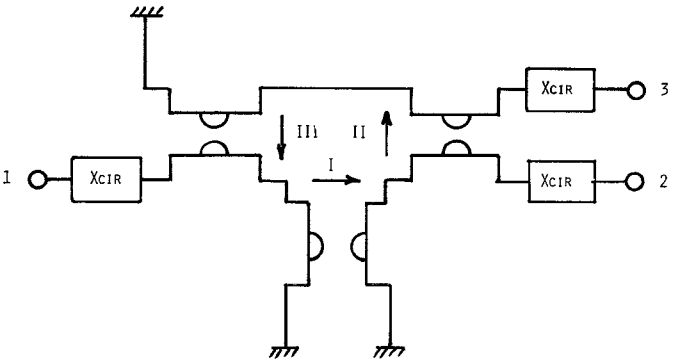

Fig. 1. Circulator model proposed by Bosma. X_{cir} is the imaginary part of Z_{cir}. The real part of Z_{cir} is the gyrator impedance of each gyrator.

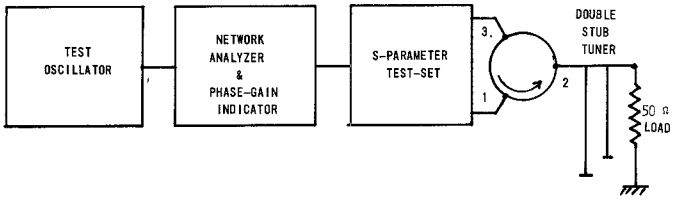

Fig. 2. Block diagram of the measuring setup for determining Z_{cir}.

An Accurate Junction Circulator Design Procedure

STEVEN J. SALAY AND HARRY J. PEPPIATT

***Abstract*—A two-step design procedure for the accurate synthesis of a junction circulator is given. The procedure is accurate to within a few decibels for isolation in the 20- to 40-dB range.**

The theory of the stripline junction circulator [1], [2] has been useful to the designer in a qualitative way, but it falls short of predicting the broad-band performance required in many applications. Bosma [3] has proposed a broad-band circulator model involving three coupled gyrators connected as shown in Fig. 1. Z_{cir} is the impedance related to the resonant modes coupled by the gyrators and the gyrator impedance, as indicated. For the stripline junction circulator, Bosma [3] has obtained the following relation for Z_{cir}:

$$\frac{1}{Z_{cir}} = 0.67\eta\left[\frac{\sqrt{3}(\kappa/\mu)}{x} - j\frac{J_1'(x)}{J_1(x)}\right]$$

$$x = \frac{2\pi R}{\lambda_0}\sqrt{\epsilon\mu_e}$$

$$\eta = 4\pi\frac{R}{W}\sqrt{\frac{\epsilon_0\epsilon}{\mu_0\mu_e}}\frac{1}{\ln\left[(W+D)/(W+T)\right]} \tag{1}$$

where

$J_1(x)$, $J_1'(x)$	first-order Bessel function and its derivative,
μ_e	effective permeability,
ϵ	dielectric constant of ferrite,
R	radius of ferrite pucks,
W, D, T	width, height, and thickness of the stripline coupled to the pucks.

A more general result applicable to microstrip and other line couplings is obtained by replacing η by η' where

$$\eta' = \frac{\pi R}{WZ_0}\sqrt{\frac{\epsilon}{\epsilon_d\mu_e}} \tag{2}$$

and

ϵ_d	effective dielectric constant of the line,
Z_0	the characteristic impedance of the line.

Bosma [3] and others [5] have indicated that the circuit of Fig. 1 gives only qualitative agreement with measured performance, especially for below resonance circulators. This correspondence is an attempt to show that the model itself is quite accurate and that discrepancies arise due to the inaccuracy in the boundary value solution for Z_{cir}. Also, a two-step design procedure for accurate circulator synthesis is given.

It is easily shown (Fig. 1) that if the complex conjugate of Z_{cir} is used as the load at port 2, ideal isolation is obtained between the driven port, port 1, and port 3. In this condition, the input impedance at port 1 is Z_{cir}. With an experimental setup[1] shown in Fig. 2 a point-by-point measurement of Z_{cir} versus frequency can be made by first adjusting the double stub tuner for maximum isolation at each frequency. Since Z_{cir} is the input impedance at the outer radius of the ferrite pucks, and from (2), one would suspect Z_{cir} to be dependent on line dimensions; the measurement should be made for a few different line couplings. The results of such measurements are shown in Fig. 3. The tuning stubs were adjusted to give isolation (port 1 to 3) of greater than 40 dB at each frequency in this octave bandwidth. Note that the measured change in Z_{cir} with the line dimension W is perhaps less than expected, a fact which facilitates the design procedure.

The experimental measurement of Z_{cir} is then used in a computer analysis program [5] (based on the model) which computes forward loss, return loss, and isolation. Arbitrary networks can be inserted at each port for matching purposes. With this program, one can optimize the performance to the specifications required.

A comparison of the computed and measured isolation of a circulator is shown as an example in Fig. 4. The measured circulator (a compact design using a dielectric ring) was fabricated directly from the data supplied by the computer program without any fine tuning. The agreement is within the accuracy associated with S parameter and time domain reflectometer equipment used in normal transmission line impedance measurements.

Manuscript received April 26, 1971; revised July 23, 1971. This correspondence is part of S. J. Salay's dissertation submitted to the Virginia Polytechnic Institute and State University, Blacksburg, Va., in partial fulfillment of the requirements for the Ph.D. degree.

The authors are with the Telecommunication Products Department, General Electric Company, Lynchburg, Va. 24502.

[1] This setup is similar to that used by Simon [4].